

Strong-stability-preserving explicit Runge-Kutta methods for SPH elastodynamics

*L. He¹, R.S. Crouch¹, M. Seaid¹ and C.E. Augarde¹

¹ School of Engineering and Computing Sciences,
University of Durham,
Durham DH1 3LE, UK

* Corresponding author: lisha.he@durham.ac.uk

Abstract

Developing an explicit time stepping scheme to accurately capture the dynamics in elastic materials is still a challenging problem. In the current study we investigate the accuracy and the stability of a family of explicit Runge-Kutta methods for the smoothed particle hydrodynamics (SPH) solution of equations in elastodynamics. The SPH method employs a purely meshless Lagrangian numerical technique for spatial discretization of the domain and it avoids many numerical difficulties related to re-meshing in mesh-based methods such as the finite element methods. The examined integration methods include the explicit Euler, explicit Runge-Kutta and explicit Runge-Kutta Chebyshev (RKC) schemes. Numerical results are presented for two test examples: shock-wave propagation in a one-dimensional problem and the velocity loading on a two-dimensional elastic plate. It is found that the proposed RKC scheme offers a robust and accurate approach for solving elastodynamics using SPH techniques.

Keywords: Elastodynamics, SPH method, explicit Runge-Kutta schemes, Numerical simulations

Introduction

The Smoothed Particle Hydrodynamics (SPH) method was first developed by Lucy [6], Gingold and Monaghan [4]. In this method, the continuum domain is discretized into particles carrying the field variables. These variables are calculated from the contribution of the neighboring particles by means of a kernel function. The SPH is a truly meshless method based on the transformation of differential equations into integral ones which are then discretized using a distribution of moving particles. The SPH method has been traditionally applied to modeling fluid flows. In recent years, there has been a growing interest in applying SPH method to a wide variety of solid mechanics problems [5]. The main feature of SPH method is that it is a particle based technique and does not require any underlying grid structure to represent the problem geometry. This avoids the difficulties associated with traditional mesh-based methods (FEM, FVM and BEM), e.g. maintaining the integrity and quality of the mesh under large deformation. The mesh-free nature of the SPH method makes this method ideally suited to modeling processes that involve large deformations and discontinuities, such as fracture and fragmentation, metal forming, etc. It has given relatively good results in many applications in both fluid and solid dynamics.

The emphasis in this work is on the time integration of the resultant system of ordinary differential equations generated from the SPH space discretization of the transient elastodynamic problem. The

examined integration methods include the explicit Euler, explicit Runge-Kutta and explicit Runge-Kutta Chebyshev (RKC) schemes. In this paper, the SPH method is first explained, in relation to the discretization of the governing equations. Thereafter, time stepping techniques are employed to integrate the semi-discrete problem. After experiments with the different time integration schemes for a transient problem with known analytical solution, accuracy and efficiency of the different schemes are discussed. Numerical results are presented for two test examples: shock-wave propagation in a one-dimensional problem and velocity loading on a two-dimensional elastic plane. It is found that the proposed RKC scheme offers a robust and accurate approach for solving elastodynamics using SPH techniques.

SPH Method in Elastodynamics

The governing equation in elastodynamics expresses of the conservation of momentum as follows

$$\frac{D\mathbf{v}}{Dt} = \frac{1}{\rho}\nabla\boldsymbol{\sigma}, \quad (1a)$$

where $\nabla = (\frac{\partial}{\partial x}, \frac{\partial}{\partial y}, \frac{\partial}{\partial z})^T$ is the gradient operator, ρ the density, \mathbf{v} the velocity, $\boldsymbol{\sigma}$ the stress tensor and $(\frac{D}{Dt} = \frac{\partial}{\partial t} + \mathbf{v} \cdot \nabla)$ is the total derivative. In our case the density is constant in time and therefore no need to consider the energy equation. The mathematical model for small strains and displacements will be employed in this study. Thus,

$$\dot{\boldsymbol{\varepsilon}} = \frac{1}{2} \left(\nabla \cdot \mathbf{v} + (\nabla \cdot \mathbf{v})^T \right), \quad \dot{\boldsymbol{\sigma}} = \mathbf{D}^e \dot{\boldsymbol{\varepsilon}}, \quad (1b)$$

where the elastic constitutive matrix is given by

$$\mathbf{D}^e = \frac{E}{(1+\nu)(1-2\nu)} \begin{bmatrix} 1-\nu & \nu & \nu & 0 & 0 & 0 \\ \nu & 1-\nu & \nu & 0 & 0 & 0 \\ \nu & \nu & 1-\nu & 0 & 0 & 0 \\ 0 & 0 & 0 & \frac{1-2\nu}{2} & 0 & 0 \\ 0 & 0 & 0 & 0 & \frac{1-2\nu}{2} & 0 \\ 0 & 0 & 0 & 0 & 0 & \frac{1-2\nu}{2} \end{bmatrix}, \quad (2)$$

and E is Young's modulus, ν is Poisson's ratio. Then we can reformulate the (1a) into another form,

$$\frac{1}{\rho}\nabla\boldsymbol{\sigma} = \nabla\left(\frac{\boldsymbol{\sigma}}{\rho}\right) + \frac{\boldsymbol{\sigma}}{\rho^2}\nabla\rho, \quad (3)$$

In the SPH method, the continuum domain Ω is discretized into a set of N particles. The field variables and its spacial gradient can be determined from the contributions from the neighbouring particles

$$f_i = \sum_{j=1}^N \frac{m_j}{\rho_j} f_j \mathbf{W}_{ij}, \quad \nabla f_i = \sum_{j=1}^N \frac{m_j}{\rho_j} f_j \nabla \mathbf{W}_{ij}. \quad (4)$$

where W_{ij} is the smoothing (kernel) function. In the present work, we use the following B-spline function [7],

$$W(R, h) = \frac{15}{7\pi h^2} \begin{cases} \frac{2}{3} - 4R^2 + \frac{1}{2}(2R)^3, & \text{if } R < \frac{1}{2}, \\ 6(2 - 2R)^3, & \text{if } 1 \leq R < 1, \\ 0, & \text{if } R > 1, \end{cases} \quad (5)$$

with h is the smoothing length and $R = \frac{|\mathbf{X}_i - \mathbf{X}_j|}{h}$.

It is clear that for the particle near boundary, the support domain will lack neighbouring particles. To overcome this drawback we correct the approximation function using the procedure proposed in [1]. The correction forms are based on the principle that the smoothing function is normalised in the support domain $\sum_{j=1}^N \frac{m_j}{\rho_j} W_{ij} = 1$. Hence,

$$f_i = \frac{\sum_{j=1}^N \frac{m_j}{\rho_j} f_j W_{ij}}{\sum_{j=1}^N \frac{m_j}{\rho_j} W_{ij}} = \sum_{j=1}^N \frac{m_j}{\rho_j} f_j \tilde{W}_{ij}. \quad (6)$$

Since $\nabla \mathbf{X}_i = \sum_{j=1}^N \frac{m_j}{\rho_j} \mathbf{X}_j \nabla W_{ij} = 1$ and $\mathbf{X}_i \sum_{j=1}^N \frac{m_j}{\rho_j} \nabla W_{ij} = \sum_{j=1}^N \frac{m_j}{\rho_j} \mathbf{X}_i \nabla W_{ij} = 0$, the equation (6) can be represented into two following forms,

$$\nabla f_i = \frac{\sum_{j=1}^N \frac{m_j}{\rho_j} f_j \nabla W_{ij}}{\sum_{j=1}^N \frac{m_j}{\rho_j} (\mathbf{X}_j - \mathbf{X}_i) \nabla W_{ij}} = \sum_{j=1}^N \frac{m_j}{\rho_j} f_j \tilde{\nabla} W_{ij}, \quad (7a)$$

$$\nabla f_i = \sum_{j=1}^N \frac{m_j}{\rho_j} (f_j - f_i) \tilde{\nabla} W_{ij}. \quad (7b)$$

Note that the second derivative of the kernel (5) is continuous, and the leading truncation error term is $\mathcal{O}(h^2)$. The finiteness of the kernel support means that only a limited number of neighbouring particles play a role in all the sums of conservation equations. This is used to reduce the computational time by building a link list between particles at each time step.

The artificial viscosity is always applied to reduce the unphysical oscillations and improve the numerical stability, which can be written as Π_{ij} . In this study we choose to apply the most popular expression of artificial viscosity which is developed by Monaghan [7],

$$\Pi_{ij} = \begin{cases} \frac{-\alpha_{\Pi} c_{ij} \phi_{ij} + \beta_{\Pi} \phi_{ij}^2}{\rho_{ij}}, & v_{ij} \cdot r_{ij} < 0, \\ 0, & v_{ij} \cdot r_{ij} \geq 0 \end{cases} \quad (8)$$

where we have $\phi_{ij} = \frac{h_{ij} v_{ij} \cdot r_{ij}}{|r_{ij}|^2 + 0.01 h_{ij}^2}$, $c_{ij} = \frac{c_i + c_j}{2}$, $\rho_{ij} = \frac{\rho_i + \rho_j}{2}$, $h_{ij} = 0.5(h_i + h_j)$, $r_{ij} = r_i - r_j$ and $v_{ij} = v_i - v_j$.

Apply the SPH discretization into the elastodynamics system, the semi-discretized equations can be reformulated in a compact SPH form

$$\frac{D}{Dt} \begin{bmatrix} v_i^x \\ v_i^y \end{bmatrix} = \begin{bmatrix} \sum_{j=1}^N m_j \left(\frac{\sigma_j^{xx}}{\rho_j^2} + \frac{\sigma_i^{xx}}{\rho_i^2} - \Pi_{ij} \right) \frac{\partial \tilde{W}_{ij}}{\partial x} + \sum_{j=1}^N m_j \left(\frac{\sigma_j^{xy}}{\rho_j^2} + \frac{\sigma_i^{xy}}{\rho_i^2} \right) \frac{\partial \tilde{W}_{ij}}{\partial y} \\ \sum_{j=1}^N m_j \left(\frac{\sigma_j^{yx}}{\rho_j^2} + \frac{\sigma_i^{yx}}{\rho_i^2} \right) \frac{\partial \tilde{W}_{ij}}{\partial x} + \sum_{j=1}^N m_j \left(\frac{\sigma_j^{yy}}{\rho_j^2} + \frac{\sigma_i^{yy}}{\rho_i^2} - \Pi_{ij} \right) \frac{\partial \tilde{W}_{ij}}{\partial y} \end{bmatrix}. \quad (9a)$$

In practice, involving the difference of velocity between two interactive particles brings more accurate results than using single neighbouring particle's velocity. Then we can apply equation (7b) on the equation (1b),

$$\frac{D}{Dt} \begin{bmatrix} \sigma_i^{xx} \\ \sigma_i^{yy} \\ \sigma_i^{xy} \end{bmatrix} = \begin{bmatrix} \sum_{j=1}^N \frac{m_j}{\rho_j} \left(D_{11}v_j^x - D_{11}v_i^x \right) \frac{\partial \tilde{W}_{ij}}{\partial x} + \sum_{j=1}^N \frac{m_j}{\rho_j} \left(D_{12}v_j^y - D_{12}v_i^y \right) \frac{\partial \tilde{W}_{ij}}{\partial y} \\ \sum_{j=1}^N \frac{m_j}{\rho_j} \left(D_{21}v_j^x - D_{21}v_i^x \right) \frac{\partial \tilde{W}_{ij}}{\partial x} + \sum_{j=1}^N \frac{m_j}{\rho_j} \left(D_{22}v_j^y - D_{22}v_i^y \right) \frac{\partial \tilde{W}_{ij}}{\partial y} \\ \sum_{j=1}^N \frac{m_j}{\rho_j} \left(D_{33}v_j^y - D_{33}v_i^y \right) \frac{\partial \tilde{W}_{ij}}{\partial x} + \sum_{j=1}^N \frac{m_j}{\rho_j} \left(D_{33}v_j^x - D_{33}v_i^x \right) \frac{\partial \tilde{W}_{ij}}{\partial y} \end{bmatrix}, \quad (9b)$$

where D_{ij} are the entries of the elastic matrix \mathbf{D} for plane stress *i.e.*, $\mathbf{D} = \frac{E}{(1-\nu^2)} \begin{bmatrix} 1 & \nu & 0 \\ \nu & 1 & 0 \\ 0 & 0 & \frac{1-\nu}{2} \end{bmatrix}$.

Strong-stability-preserving explicit Runge-Kutta methods

The solution procedure for equations (9) is completed when a time integration of the semi-discrete SPH equations is selected. This stage can be handled by any implicit ordinary differential equation (ODE) solver, since they are computationally without risk by virtue of their accuracy and linear unconditionally stability. This allows for larger time steps in the integration process. However, due to the large set of linear system of algebraic equations at each time step, these methods may be computationally inefficient. As an alternative, we use a class of explicit Runge-Kutta methods. Applied to the system (9), the SPH discretization can be reformulated in a compact system of ODE of this form

$$\frac{d\mathbf{U}}{dt} = \mathbf{F}(\mathbf{U}), \quad t \in (0, T], \quad (10)$$

where $\mathbf{U} = [\sigma_{xx} \ \sigma_{yy} \ \sigma_{xy} \ v_x \ v_y]^T$ and the right-hand side $\mathbf{F}(\mathbf{U})$ is defined accordingly to (9). It should be stressed that, because explicit time stepping schemes evaluate explicitly the right-hand side of the equation (10), then it has to satisfy a stability condition. This stability criterion can be reached based on the Courant-Friedrichs-Levy (CFL) condition

$$c \frac{\Delta t}{\Delta x} \leq 1, \quad (11)$$

where $c = \sqrt{\frac{E}{\rho}}$ is the wave speed and Δx is the initial spacing between two particles. Difficulties often appear when the spectral radius of the Jacobian of \mathbf{F} , $\partial\mathbf{F}/\partial\mathbf{U}$, has large eigenvalues. This may give rise to numerical stiffness. Thus, time integration schemes for (10) depend strongly on the spectral radius $\rho(\partial\mathbf{F}/\partial\mathbf{U})$ and grid refinements, and for these reasons it is preferable that these schemes have to be either implicit or explicit with large stability regions. In the current work, we consider the RKC method studied for example in [2, 8, 3]. The RKC method has been designed for explicit time integration of systems of parabolic equations. To solve (10) the RKC scheme takes the

form

$$\begin{aligned}
\mathbf{U}^{(0)} &= \mathbf{U}^n, \\
\mathbf{U}^{(1)} &= \mathbf{U}^{(0)} + \tilde{\mu}_1 \mathbf{F}^{(0)} \\
\mathbf{U}^{(j)} &= \mu_j \mathbf{U}^{(j-1)} + \nu_j \mathbf{U}^{(j-2)} + (1 - \mu_j - \nu_j) \mathbf{U}^{(0)} + \tilde{\mu}_j \mathbf{F}^{(j-1)} + \tilde{\gamma}_j \mathbf{F}^{(0)}, \quad 2 \leq j \leq s, \\
\mathbf{U}^{n+1} &= \mathbf{U}^{(s)},
\end{aligned} \tag{12}$$

where \mathbf{U}^n is the solution computed at time step t_n , $\mathbf{F}^{(j)}$ denotes the term $\mathbf{F}(t_n + c_j \Delta t, \mathbf{U}^{(j)})$ and $\mathbf{U}^{(j)}$ are internal vectors for RKC stages. The coefficients in (12) are available in analytical form for arbitrary $s \geq 0$ from [2, 8]. For convenience of the reader we include the formulae for these coefficients. Consider the Chebyshev polynomial of the first kind of degree j

$$T_j(z) = \cos(j \arccos z), \quad -1 \leq z \leq 1.$$

Then

$$\begin{aligned}
\epsilon &= \frac{2}{13}, \quad q_0 = 1 + \frac{\epsilon}{s^2}, \quad q_1 = \frac{T'_s(q_0)}{T''_s(q_0)}, \\
b_j &= \frac{T''_j(q_0)}{(T'_j(q_0))^2}, \quad (2 \leq j \leq s), \quad b_0 = b_2, \quad b_1 = b_2,
\end{aligned}$$

and

$$\begin{aligned}
\tilde{\mu}_1 &= b_1 q_1, \quad \mu_j = 2q_0 \frac{b_j}{b_{j-1}}, \quad \nu_j = -\frac{b_j}{b_{j-2}}, \quad \tilde{\mu}_j = 2q_1 \frac{b_j}{b_{j-1}}, \\
\tilde{\gamma}_j &= (1 - b_{j-1} T_{j-1}(q_0)) \tilde{\mu}_j, \quad (2 \leq j \leq s).
\end{aligned}$$

The coefficients c_j are

$$c_j = \frac{T'_s(q_0)}{T''_s(q_0)} \frac{T''_j(q_0)}{T'_j(q_0)} \approx \frac{j^2 - 1}{s^2 - 1} \quad (2 \leq j \leq s), \quad c_1 = \frac{c_2}{T'_2(q_0)} \approx \frac{c_2}{4}, \quad c_s = 1.$$

It should be pointed out that two criteria have been taken into consideration for the calculation of the above coefficients namely, (i) the real stability boundary, $\beta(s)$, has to be as large as possible to obtain good stability properties for parabolic equations, and (ii) the application of the method with arbitrary number of stages should not damage the convergence properties, that is, the accumulation of local errors does not grow without bound. Observe that the number of stages s in our SPH method and the conventional RKC scheme varies with Δt such that, see [8],

$$s = 1 + \left\lceil \sqrt{1 + \frac{c \Delta t}{0.653 \Delta x}} \right\rceil, \tag{13}$$

where $\lceil x \rceil$ denotes the integer part of x and $c = \sqrt{\frac{E}{\rho}}$ is the wave speed.

Numerical results

We then examine the performance of the proposed time stepping schemes for SPH method for a class of elastic problems in one and two dimensions. In the first example we solve the problem of propagation of a shock wave on a one dimensional elastic magnesium bar and the second example solve a large deformation problem in two dimensional elastic magnesium plate.

One-dimensional shock-wave propagation

In this example we solve the problem of propagation of a shock wave on one-dimensional magnesium bar. The length of the bar $L = 1m$ with material properties of $\rho = 1738 \text{ kg/m}^3$ and the Young's modulus $E = 45 \times 10^9 \text{ Pa}$. Initial the bar is at rest with $v = 0$ and $\sigma = 0$. The velocity at the right end of the bar is fixed ($v = 0$) and we apply a compression stress on the left boundary $\sigma_0 = 8.8436 \times 10^6 \text{ Pa}$. The analytical velocity of the shock wave in this problem could be easily calculated by $v_0 = \sigma_0/\sqrt{E\rho} = 1 \text{ m/s}$. The wave will propagate through the bar with the wave speed $c = \sqrt{E/\rho} = 5.0884 \times 10^3 \text{ m/s}$. When the wave arrives the fixed right end of the bar, the stress at this point will double to become $17.6872 \times 10^6 \text{ Pa}$. In Figure 1(a), 1(b), 1(c) and 1(d), we

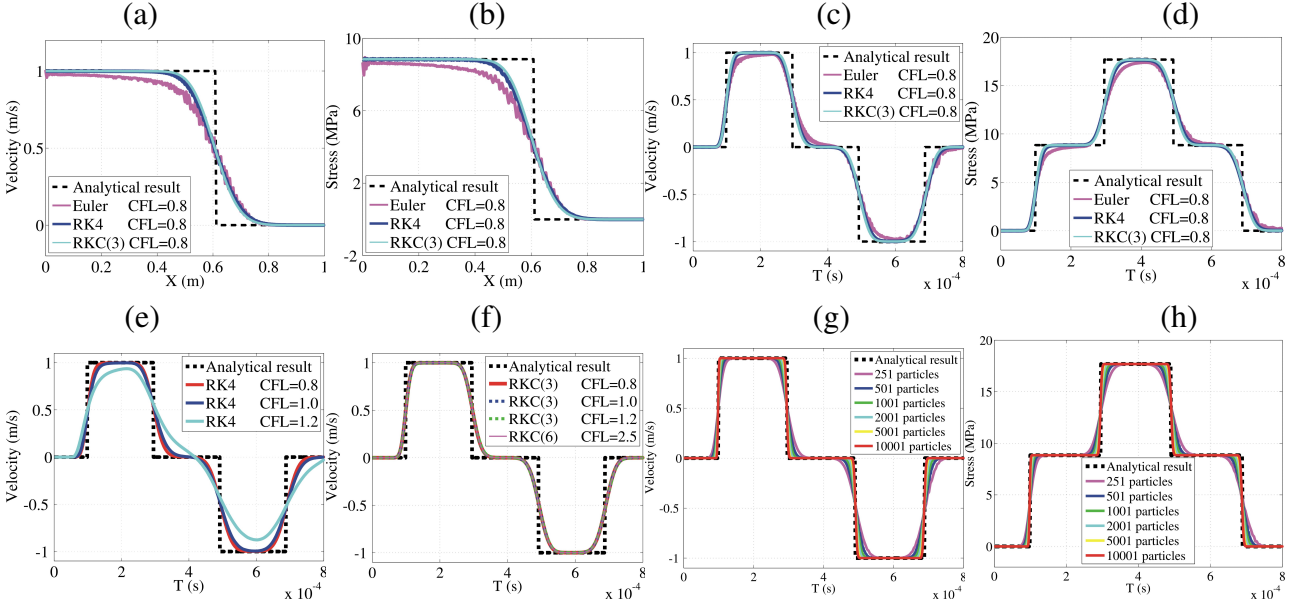


Figure 1: Numerical results for the shock-wave propagation problem.

present the velocity and the stress along the bar at time $t = 1.2 \times 10^{-3} \text{ s}$ and the time evolution of velocity and stress at the mid point of the bar ($x = L/2$), obtained using the considered time stepping schemes and 251 particles. It is evident from these results that the RKC scheme with 3 stages produces more stable and accurate results than the other considered schemes. As we know, the stability will decrease while increasing the value of CFL in normal time stepping schemes, like the RK4 scheme shown on Figure 1(e). However, Figure 1(f) shows that the RKC scheme can still present stable results with a larger value of CFL in condition with increasing number of stages. To further examine the convergence of the RKC scheme applied in the SPH method, we then apply the RKC scheme with more particles, as shown on Figure 1(g) and 1(h). The error rates of using the SPH method for solving Example 1 with different time schemes are shown on Table 1, the error rate is obtained from the equation,

$$error_1 = \frac{\sum |u^{SPH} - u^{exact}|}{\sum |u^{exact}|}.$$

Two-dimensional elastic plane

As a second example we consider a two-dimensional version of the previous example solved in the computational domain shown in Figure 2. The material properties of the plane are $\rho = 2000 \text{ kg/m}^3$,

Table 1: Error rate of using the SPH method for solving Example 1 with different time schemes.

# nodes	CFL = 0.8			CFL=1.0			CFL=2.5		
	Euler	RK4	RKC	Euler	RK4	RKC	Euler	RK4	RKC
251	0.2417	0.1866	0.1661	-	0.2313	0.1655	-	-	0.1655
501	0.1676	0.1306	0.1165	-	0.1616	0.1165	-	-	0.116
1001	0.1157	0.092	0.082	-	0.1135	0.0821	-	-	0.0815
2001	0.0747	0.0651	0.0579	-	0.0802	0.0579	-	-	0.0574

the Youngs modulus $E = 80 \times 10^6 Pa$ and the Poisson ratio $\nu = 1/3$. Fixed boundary conditions are applied on the upper and right sides of the plane, whereas, the velocity on the lowest left circular boundary is given as

$$v(t) = \begin{cases} 5 \text{ m/s}, & \text{if } t \leq 1.8 \times 10^{-3} \text{ s}, \\ 0 \text{ m/s}, & \text{otherwise.} \end{cases}$$

Based on the observations drawn from the previous example, we present numerical results obtained using the RKC scheme. We also examine the performance of our SPH method for three different node distributions exhibited in Figure 2. The corresponding node statistics along with the time steps used for each nodal distribution are summarized in Table 2. In this table we also include the minimum and maximum values of the principal stress obtained for the considered nodal distributions and a reference solution obtained on a very fine SHP nodal distribution.

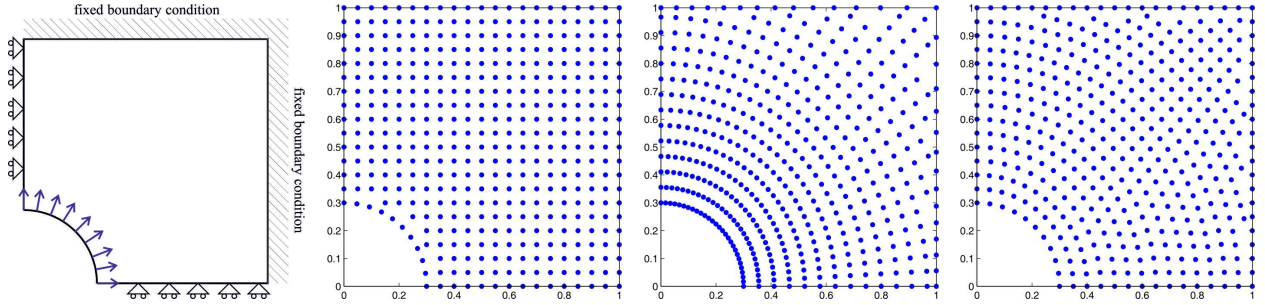


Figure 2: Computational domain and node collocations for Example 2.

Table 2: Nodal statistics and results for the principal stresses obtained using the SPH method for solving Example 2.

	# nodes	Δt	$t = 0.0018 \text{ s}$		$t = 0.003 \text{ s}$		$t = 0.0048 \text{ s}$	
			max σ_p	min σ_p	max σ_p	min σ_p	max σ_p	min σ_p
Reference	24170	1.25e-5	3.01e+6	0	1.87e+6	-1.26e+5	2.86e+6	-1.50e+6
Equal radial	2446	1.20e-4	2.95e+6	0	1.96e+6	-2.60e+5	2.96e+6	-1.96e+6
Uniform	2423	1.20e-4	3.23e+6	0	1.93e+6	-2.83e+5	2.64e+6	-3.83e+5
Radial	2376	1.19e-4	2.99e+6	0	1.64e+6	-1.21e+5	2.72e+6	-3.14e+5

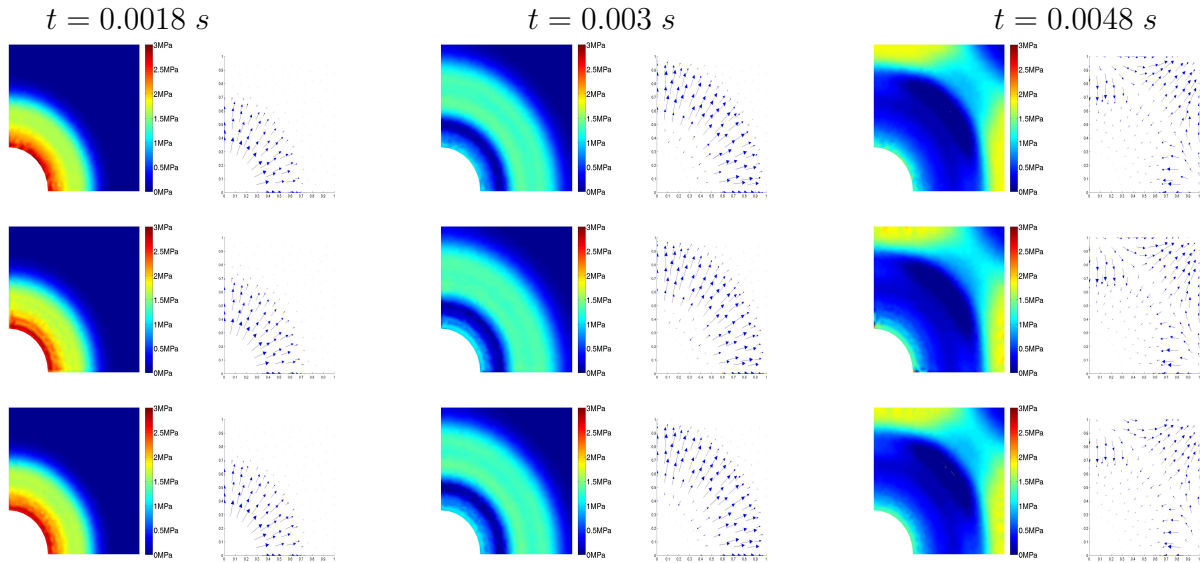


Figure 3: Stress distributions and velocity fields obtained for different node collocations and at three different simulation times. Uniform distribution (first row), radial distribution (second row) and equally radial distribution (third row).

In Figure 3 we present the stress distributions and velocity fields obtained for different node collocations and at three different simulation times namely $t = 0.0018\text{ s}$, $t = 0.003\text{ s}$ and $t = 0.0048\text{ s}$. At early simulation times, a shock wave is generated and propagates along the main diagonal in the computational domain. Reflections from fixed boundaries in the domain are also captured by the SPH method for all the considered nodal distributions. The reflection features are more visible in the velocity fields than the stress distributions at $t = 0.0048\text{ s}$. From the presented results it is evident that the nodal distribution in the considered SPH method affects quantitatively and qualitatively the simulated results. The artificial viscosity has been considered in all the analysis of example 2. It seems that, for the considered material properties and the boundary conditions, at the early stage $t = 0.0018\text{ s}$, the SPH method using the radial and equally radial nodal distributions produces more accurate results in term of both stress and velocity fields, because the distances between two nearest neighbouring particles near the curve boundary are similar in these two distributions, which bring more reasonable results. When the wave propagates to the fixed boundary and reflects ($t = 0.0048\text{ s}$), the uniform distribution brings smoother results than others in terms of both stress and velocity, because the the distances between two nearest neighbouring particles near the fixed boundary are similar in uniform distribution, which can brings more accurate results.

References

- [1] J. Bonet and S. Kulasegaram. Correction and stabilization of smooth particle hydrodynamics methods with application in metal forming simulations. *Int. J. Numer. Methods Eng*, 47:1189–1214, 2000.
- [2] P.J. Van der Houwen. Explicit Runge-Kutta formulas with increased stability boundaries. *Numer. Math.*, 20:149–164, 1972.

- [3] P.J. Van der Houwen and B.P. Sommeijer. On the internal stability of explicit, m-stage Runge-Kutta methods for large m-values. *Z. Angew. Math. Mech.*, 60:479–485, 1980.
- [4] R. A. Gingold and J. J. Monaghan. Smoothed particles hydrodynamics: theory and application to non-spherical stars. *Monthly Notices of the Royal Astronomical Society*, 181:375–389, 1977.
- [5] M. B. Liu and G. R. Liu. Smoothed particle hydrodynamics (sph): an overview and recent developments. archives of computational methods in engineering. *Monthly Notices of the Royal Astronomical Society*, 17(1):25–76, 2010.
- [6] L. B. Lucy. A numerical approach to the testing of the fission hypothesis. *Astronomical Journal*, 82(12):1013–1024, 1977.
- [7] J. J. Monaghan. Smoothed particle hydrodynamics. *Astro. Astrophys*, 30:543–574, 1992.
- [8] J.G. Verwer, W.H. Hundsdorfer, and B.P. Sommeijer. Convergence properties of the Runge-Kutta-Chebyshev method. *Numer. Math.*, 57:157–178, 1990.